Strain induced enhancement of perpendicular magnetic anisotropy in Co/graphene and Co/BN heterostructures

B. S. Yang,[1,2] J. Zhang,[3] L. N. Jiang,[2] W. Z. Chen,[2] P. Tang,[2] X.-G. Zhang,[4] Y. Yan,[1,*] and X. F. Han[2,†]

[1]*Key Laboratory of Physics and Technology for Advanced Batteries (Ministry of Education), Department of Physics, Jilin University, Changchun 130012, People's Republic of China*

[2]*Beijing National Laboratory for Condensed Matter Physics, Institute of Physics, University of Chinese Academy of Sciences, Chinese Academy of Sciences, Beijing 100190, China*

[3]*School of Physics and Wuhan National High Magnetic Field Center, Huazhong University of Science and Technology, 430074 Wuhan, China*

[4]*Department of Physics and the Quantum Theory Project, University of Florida - Gainesville, Florida 32611, USA*

(Received 22 January 2017; revised manuscript received 26 March 2017; published 17 May 2017)

Perpendicular magnetic tunnel junctions in the next-generation magnetic memory using current induced magnetization switching will likely rely on a material design that can enhance the perpendicular magnetic anisotropy of heterojunctions containing only light elements. Using first-principles calculations, we investigated the effect of compressive and tensile strain on the perpendicular magnetic anisotropy of light element heterostructures of Co films, Co/graphene, and Co/BN. We found that the perpendicular magnetic anisotropy of Co/graphene is greatly enhanced compared to the Co films, while that of Co/BN is reduced compared to the Co films. In addition, tensile strain can further enhance perpendicular magnetic anisotropy of Co/graphene and Co/BN heterojunctions by 48.5% and 80.8%, respectively, compared to the unstrained systems. A density of state analysis, combined with layer and orbital magnetic anisotropy contributions obtained from a second-order perturbation theory of the spin-orbit coupling, reveals that the tensile strain effect arises from the increase of the hybridization between same spin d_{xy} and $d_{x^2-y^2}$ states of the surface Co film. Our results suggest that strain engineering is an effective approach to enhance the perpendicular magnetic anisotropy of light element heterostructures.

DOI: 10.1103/PhysRevB.95.174424

I. INTRODUCTION

The perpendicular magnetic tunnel junction (p-MTJ), in which the magnetic moments of the ferromagnetic electrodes are aligned perpendicular to the junction layers, is the basis for spin transfer torque magnetoresistive devices that have the properties of high-density nonvolatile memory, high thermal stability, and low critical current. These properties are some of the essential requirements for the next-generation current induced magnetization switching magnetic memory [1–4]. The common approach for generating large perpendicular magnetic anisotropy (PMA) for a free layer is to use heavy metal (HM) elements or capping with a HM multilayer [5–13]. However, adding a noble metal element increases the magnetic damping constant due to its large spin-orbital coupling, and thus can be detrimental to low critical switching current [14,15]. The spin-orbital coupling strength in 3*d* ferromagnetic metals (FM) and their oxides is usually $2 \sim 3$ times smaller than that of HMs or HM multilayer materials [12]. Therefore a light element p-MTJ that can achieve PMA is more desirable. How to enhance the PMA in light element heterojunctions is a pressing problem for the next-generation magnetic memory.

In the past, aside from introducing noble metals in an ordinary MTJ, other solutions such as surface charging, applying an electric field, varying the composition of the alloy, adding substitution atoms in the electrode, and adding small transition metal molecules to the surface have also been used to enhance the PMA [16–31]. The mechanism of the enhanced PMA by these solutions is attributed to the change of electronic structure, especially the change of electronic states near the Fermi level [22,24,32,33]. Recent work [34,35] reported PMA as large as ~60 meV in single 3*d* transition metal Co atoms bound to MgO, where the large PMA is associated to the dominating axial ligand field on the O adsorption site. It is noticed that the PMA of Co films is enhanced by graphene due to the strong hybridization between Co and the substrate [36–39]. Particularly, Yang *et al.* showed that the PMA of Co films was doubled by graphene (Gr) coating [40]. Thus using interfaces with other light element materials, a considerable PMA can be obtained in 3*d* metals.

Strain can be an effective way to modulate the electronic structure and it has been commonly used in the ABO_3 compounds [41–43]. Therefore strain manipulation of magnetic anisotropy energy (MAE) is an attractive possibility. More importantly, it was experimentally demonstrated that compressive strain, which is considered to modify the crystal-field splitting, can rotate the easy axis of the magnetic moment of $CoCr_2O_4$ epitaxial thin films, which is pointing to the out-of-plane direction [44]. In addition, tensile strain can make the MAE of $CoFe_2O_4$ and $NiFe_2O_4$ favor the out-of-plane orientation [45], due to the crystal field splitting modified by strain. Separately, strain engineering of voltage-controlled perpendicular magnetic anisotropy in Ta/Fe/MgO and Ta/CoFe/MgO heterostructures was proposed in theoretical studies but without addressing its mechanism [33,46]. The MAE of a heterostructure depends on the electronic structure of its interfaces, the orbital moments, and the exchange splitting strength [47–50]. Strain impacts the MAE by changing the atomic spacing, which in turn changes the way the atomic orbitals overlap. For this reason,

*yanyu@jlu.edu.cn
†xfhan@iphy.ac.cn

understanding strain effects on the MAE requires a careful analysis of orbital dependent contributions. In addition, a detailed study of perpendicular anisotropy may provide a feasible avenue for searching candidate materials for spintronics applications.

In this paper, using first-principles calculations, we study the effect of strain on the MAE of hcp-Co multilayers on graphene and BN heterostructures. By analyzing the structure, density of states, and the layer- and orbital-resolved MAE based on the second-order perturbation theory, we investigated the MAE and the influence of the strain on the MAE of Co/Gr and Co/BN heterostructures and found that the MAE is associated to the electronic structure variation, especially the d_{xy} and $d_{x^2-y^2}$ orbitals around the Fermi level.

II. COMPUTATIONAL METHODOLOGY

A. Lattice and electronic structure

All calculations were performed within the framework of density functional theory (DFT) implemented in the Vienna *ab initio* simulation package (VASP) [51–53]. The exchange-correlation potential was treated with the generalized gradient approximation with the Perdew-Burke-Ernzerhof functional [54]. The ion-electron interaction was described by the projector-augmented plane-wave (PAW) potentials [55]. The compressive strain may cause greater interlayer distances leading to a van der Waals interaction between the layers, which was treated by the vdW-DF with the OPTB88 exchange functional method [56,57]. A 15-Å vacuum region in the direction normal to the layers was used to avoid interaction between the periodic replicas such that the total energy was converged to within 0.1 meV. The convergence test for the cutoff energy shows that a 500-eV plane-wave basis set is sufficient to converge the total energy to the required accuracy. In all calculations, considering the accuracy and efficiency we used a Γ-centered $23 \times 23 \times 1$ k-point grid, which makes the MAE to converge within 0.005 meV.

Due to small lattice mismatch between Co and Gr (BN), the in-plane lattice parameter of $a = 2.46$ Å for graphene [58] and $a = 2.50$ Å for BN [59] was used for the lattice parameter in unstrained Co/Gr and Co/BN heterojunctions, respectively. In calculations for strained heterojunctions, a uniform strain was applied to all of the layers in each heterojunction. The strain is defined as $\varepsilon = (a - a_0)/a_0$ [60,61], where a and a_0 are the strained and unstrained lattice constants, respectively. For each strain, all atoms in the heterojunction were fully relaxed with a fixed in-plane lattice constant until the force on each atom is less than 0.001 eV Å^{-1} and the change in total energy between two ionic relaxation steps is smaller than 10^{-7} eV. The side and top views of Co/Gr heterostructures are shown in Fig. 1. Among them, the top1 configuration with the interface Co atom (Co_1) on top of C atom and the second layer Co (Co_2) on the hollow site of graphene is the most energetically favorable configuration [62].

B. Calculation of MAE

Following past calculations of multilayer materials, the MAE is calculated using the force theorem approach [63,64]. In this approach, a self-consistent calculation without the spin-orbital coupling is first performed to obtain the charge density of the ground state of the system. Using this charge density as input, the spin-orbital coupling is treated as a perturbation in non-self-consistent calculations of two different magnetization directions. The MAE is defined as the energy difference between the out-of-plane (perpendicular to the interface) and the in-plane directions. To remove the ambiguity about which in-plane direction to choose, we calculated the total energies for magnetization along five in-plane high-symmetry directions: [100], [210], [110], [−120], and [010], and found that the energy for all five in-plane directions is identical. Hence, in the following study, the [100] axis is chosen to be the in-plane direction of magnetization. The shape anisotropy caused by dipole-dipole interactions is not included in our spin-density-based first-principles calculations. Due to large exchange splitting, the majority-spin d states of Co atoms in Co(4 ML)/Gr and Co(4 ML)/BN heterostructures are almost fully occupied. This means that the contribution to the MAE from the SOC between unoccupied majority-spin d states and occupied majority- or minority-spin d states can be neglected. With this simplification, following the recipe of second-order perturbation theory by Wang *et al.* [65], the MAE is approximately equal to the sum of the following two terms:

$$\begin{aligned}\Delta E^{--} &= E^{--}(x) - E^{--}(z) \\ &= \xi^2 \sum_{o^-,u^-} \frac{|\langle o^-|L_z|u^-\rangle|^2 - |\langle o^-|L_x|u^-\rangle|^2}{E_u^- - E_o^-}, \qquad (1)\\ \Delta E^{+-} &= E^{+-}(x) - E^{+-}(z) \\ &= -\xi^2 \sum_{o^+,u^-} \frac{|\langle o^+|L_z|u^-\rangle|^2 - |\langle o^+|L_x|u^-\rangle|^2}{E_u^- - E_o^+}, \qquad (2)\end{aligned}$$

where ξ is the SOC constant, + and − are majority and minority spin states, u and o are the energy levels of the unoccupied states and the occupied states, respectively. According to Eqs. (1) and (2), the MAE is determined by the spin-orbital matrix element differences as well as their energy differences. The matrix element differences, $|\langle o^-|L_z|u^-\rangle|^2 - |\langle o^-|L_x|u^-\rangle|^2$ and $|\langle o^+|L_z|u^-\rangle|^2 - |\langle o^+|L_x|u^-\rangle|^2$, in Eqs. (1) and (2) are listed in Table I for the d orbitals. This expression allows one

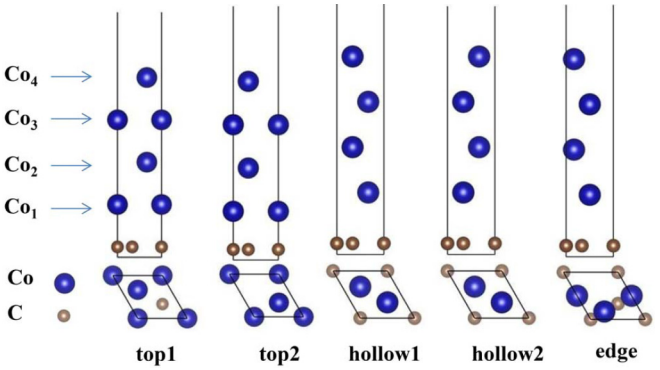

FIG. 1. Top and side views of five possible configurations of a Co(4 ML)/Gr heterostructure. Blue and brown balls represent Co and C atoms, respectively.

TABLE I. The matrix element differences between two directions of the magnetization in Eqs. (1) and (2) ($|\langle o^-|L_z|u^-\rangle|^2 - |\langle o^-|L_x|u^-\rangle|^2$ and $|\langle o^+|L_z|u^-\rangle|^2 - |\langle o^+|L_x|u^-\rangle|^2$).

	o^+					o^-				
u^-	d_{xy}	d_{yz}	d_{z^2}	d_{xz}	$d_{x^2-y^2}$	d_{xy}	d_{yz}	d_{z^2}	d_{xz}	$d_{x^2-y^2}$
d_{xy}	0	0	0	−1	4	0	0	0	1	−4
d_{yz}	0	0	−3	1	−1	0	0	3	−1	1
d_{z^2}	0	−3	0	0	0	0	3	0	0	0
d_{xz}	−1	1	0	0	0	1	−1	0	0	0
$d_{x^2-y^2}$	4	−1	0	0	0	−4	1	0	0	0

to analyze the contribution to the MAE on an orbital by orbital basis, allowing further insights to the understanding.

Equations (1) and (2) mean that the orbitals close to the Fermi energy contribute the most to MAE. It also indicates that the contributions to MAE from the same spins and from the opposite spins between occupied and unoccupied states have opposite signs. Positive and negative MAEs mean that the easy magnetization axis is perpendicular and parallel to the interface of the heterostructure, respectively.

III. RESULTS AND DISCUSSION

A. Structure and layer influence on the MAE

Figure 2(a) shows the values of MAE of unstrained Co films, and Co/Gr and Co/BN heterostructures with the thickness of the Co layer varying in the range of 2–8 monolayers (ML). The results reveal that graphene greatly enhances the MAE of Co films. The one exception is the case of 3 ML Co, in which the second Co layer has a large in-plane anisotropy, partially canceling the large perpendicular anisotropy from the interface [40]. These trends are similar to previous results. The MAE of Co/BN heterostructure is smaller than that of Co films except for films with 2 ML Co. The results for both systems can be understood in terms of bonding between the Co layer and graphene or BN as we discuss below.

Figures 2(b) and 2(c) plot the MAE as a function of tensile and compressive strains in Co/Gr and Co/BN, respectively. In view of the increased CPU time needed for systems containing more atoms, we only investigated the dependence of the MAE on the strain in Co(2–5 ML)/Gr and Co(2–5 ML)/BN heterostructures. For both heterostructures, there is a sudden drop of the MAE under a compressive strain between 1% and 2%, accompanied by a sudden increase in the distance (from ∼2 to ∼4 Å) between the interface Co atom (Co_1) and the graphene or BN layers, as shown in Figs. 2(e) and 2(f). At 4 Å, there is no bonding between Co_1 and graphene (or BN), and only the van der Waals interaction is present between these two layers. Indeed, the MAEs of Co/Gr and Co/BN under the compressive strain when the interface distance is about 4 Å are almost the same as that of Co films. This is the first piece of evidence that bonding between Co and graphene (or BN) is key to the increase in the MAE.

If bonding between Co and graphene or BN is important, then one expects that tensile strain, which decreases the interlayer distance, can also enhance the MAE of Co/Gr and Co/BN heterostructures. This is exactly what we see in Fig. 2. The MAE of representative Co(4 ML)/Gr and Co(4 ML)/BN under 5% tensile strain is enhanced by 48.5% and 80.8% compared to the unstrained systems, respectively. The layer-resolved MAE in Fig. 3(a) shows that the contribution from Co_1 in Co(4 ML)/Gr heterostructure decreases as the tensile strain is increased, while the contribution from other Co layers increases with the tensile strain. The difference can be traced to the orbital energy levels that shift with the strain and the matrix element differences in Table I as we will discuss later.

Different from Co(4 ML)/Gr, the contribution from Co_1 in Co(4 ML)/BN does not dramatically change under tensile

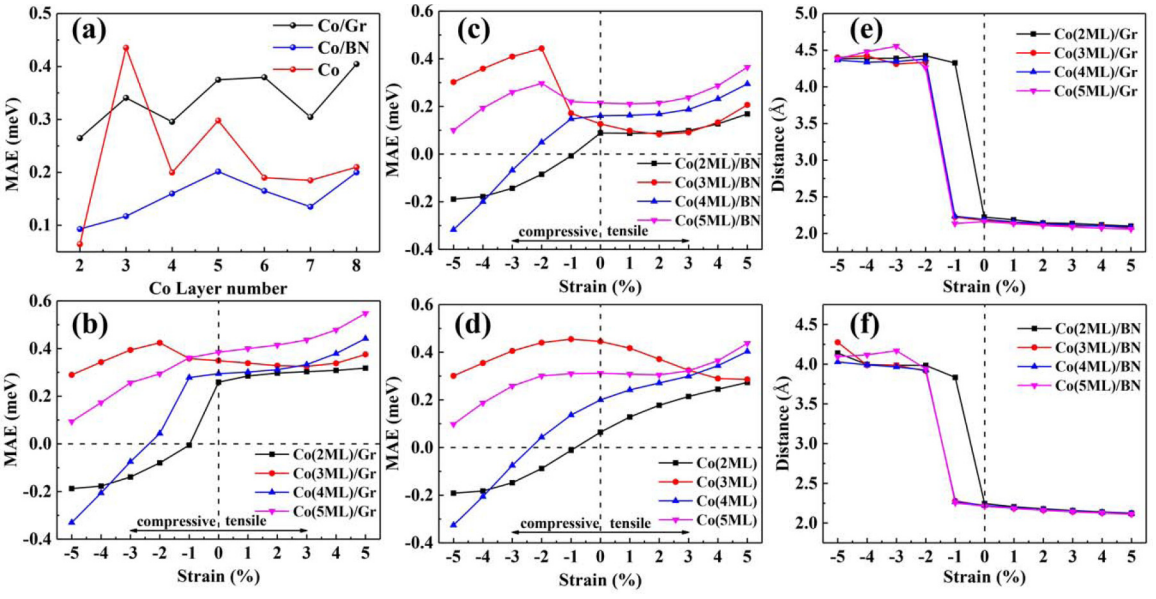

FIG. 2. (a) MAE of Co multilayer, Co/Gr and Co/BN as a function of Co layer number from 2 to 8 ML. (b), (c), and (d) MAE of Co(2–5 ML)/Gr, Co(2–5 ML)/BN, and Co(2–5 ML) multilayers as a function of strain from −5% to 5%. (e) and (f) Distance between two adjacent layers at the interface of Co/Gr and Co/BN as a function of strain.

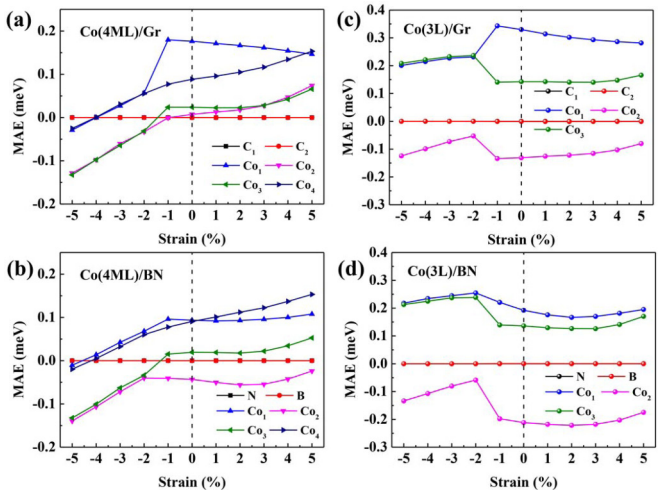

FIG. 3. Layer-resolved MAE of (a) Co(4 ML)/Gr, (b) Co(4 ML)/BN, (c) Co(3 ML)/Gr, and Co(3 ML)/BN under various strains from −5% to 5%.

strain and the contribution from Co_2 in Co(4 ML)/BN under tensile strain is negative, as shown in Fig. 3(b). Moreover, it can be seen from the layer-resolved MAE in Figs. 3(a) and 3(b) that C, B, and N atoms do not contribute to the MAE under any strains and that the interface Co (Co_1) and fourth layer Co (Co_4) in Co(4 ML)/Gr and Co(4 ML)/BN contribute the most to the MAE. Besides, the interface and outer layer Co also contribute most to MAE in other heterostructures (see Figs. 3(c) and 3(d) and Ref. [40]). The correlation to the interlayer distance indicates that the key role in the enhancement of MAE under tensile strain may be the bonding between Co and graphene or BN.

For Co(4 ML)/BN, the calculated DOS as well as layer and d-orbital resolved MAE show that the underlying mechanism of MAE enhanced by tensile strain is similar to that of Co/Gr. Figure 3 shows that the MAE of Co_1 in unstrained Co(4 ML)/BN is smaller than that in Co(4 ML)/Gr. Figure 6(a) and 6(b) show that the bonding between Co_1 and N atom is weaker than that between Co_1 and C atoms. The weaker bonding between Co_1 and N reverses the order of the energy level of the majority d_{z^2} and $d_{xy(x^2-y^2)}$ orbitals compared to that of Co_1 in Co/Gr.

B. Orbital resolved contributions

Figure 4 shows the d-orbital resolved MAE of Co_1 and Co_4 in unstrained and 5% tensile strain configurations calculated from Eqs. (1) and (2). It can be seen that the main contributions from Co_1 in unstrained Co(4 ML)/Gr are due to the matrix element differences between d_{xy} and $d_{x^2-y^2}$ orbitals as well as d_{yz} and d_{z^2} orbitals and both contributions are positive. In contrast to Co_1, although the contributions from Co_4 in unstrained Co(4 ML)/Gr due to the matrix element differences between d_{xy} and $d_{x^2-y^2}$ orbitals also show large positive values, those due to the matrix element differences between d_{yz} and d_{z^2} orbitals are negative, as shown in Fig. 4(c), leading to a smaller overall contribution from Co_4 than from Co_1. It can be seen from Figs. 5(a) and 5(c) that the energy difference between $d_{z^2}^{o+}$ and d_{yz}^{u-} states for Co_1 [labeled as Δ_1^{+-} in Fig. 5(a)] is smaller than the corresponding energy difference for Co_4 [Δ_4^{+-} in Fig. 5(c)]. The reverse is true for the $d_{z^2}^{o-}$ and d_{yz}^{u-} states, the energy difference [Δ_4^{--} in Fig. 5(c)] for Co_4 is smaller than the energy difference [Δ_1^{--} in Fig. 5(a)] for Co_1. Therefore, for matrix elements between d_{yz} and d_{z^2}, Eq. (2) contributes the most to Co_1 and Eq. (1) contributes the most to Co_4. The same spin [Eq. (1)] and the opposite spin [Eq. (2)] contributions between d_{yz} and d_{z^2} orbitals have opposite signs according to Table I. This explains why the matrix element differences between d_{yz} and d_{z^2} orbitals from Co_1 and Co_4 offer opposite contributions. The result also means that the MAE contribution from opposite spins also plays an important role.

For Co_4, 5% tensile strain decreases the coupling between the atoms in the same layer, bringing the bonding and antibonding states closer to each other in energy [see Figs. 5(a) and 5(b)]. As a result, the energy difference between the occupied and unoccupied d states becomes smaller. According to Eq. (2), this causes the contribution from the corresponding matrix element differences to the MAE to become larger

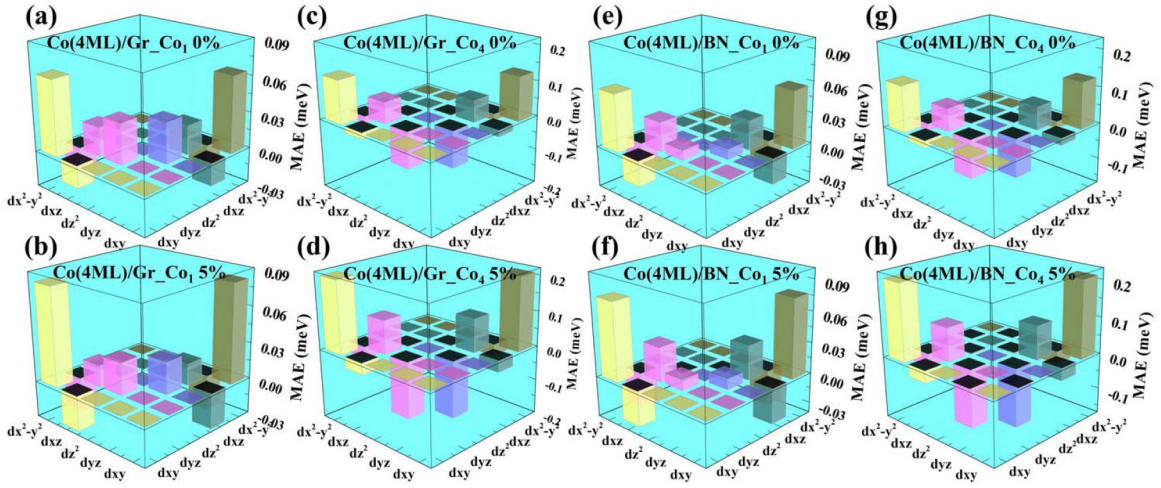

FIG. 4. d-orbital resolved MAE of Co_1 and Co_4 in unstrained Co(4 ML)/Gr and Co(4 ML)/BN as well as Co_1 and Co_4 in Co(4 ML)/Gr and Co(4 ML)/BN under 5% tensile strain.

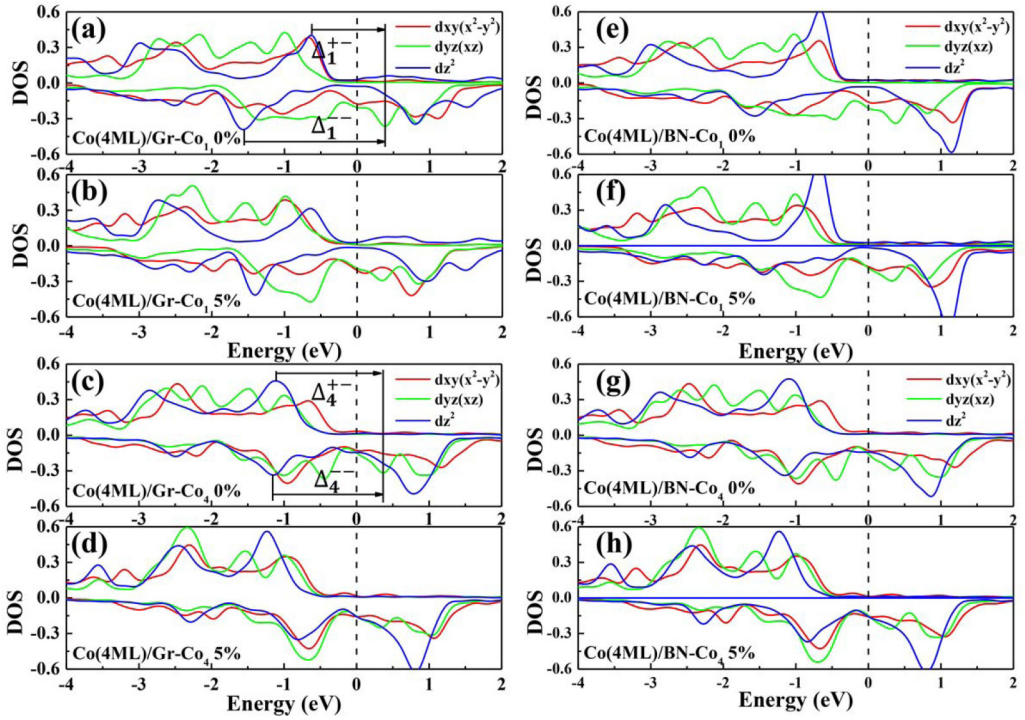

FIG. 5. The density of states of Co_1 and Co_4 in unstrained Co(4 ML)/Gr and Co(4 ML)/BN as well as Co_1 and Co_4 in Co(4 ML)/Gr and Co(4 ML)/BN under 5% tensile strain. Red, green, and blue lines represent d_{xy} and $d_{x^2-y^2}$ orbitals, d_{yz} and d_{xz} orbitals, and d_{z^2} orbital.

regardless of its sign. From the matrix element differences in Table I, we can deduce that the energy difference coming from same spin d_{xy} and $d_{x^2-y^2}$ is 4, which is the largest positive value. Therefore the MAE contribution from Co_4 increases under a tensile strain. Similar to Co_4, the MAE of Co_2 and Co_3 in Co(4 ML)/Gr also increases under a tensile strain. For Co_1, the energy difference between $d_{z^2}^{u-}$ and d_{yz}^{o-} as well as d_{xz}^{o-} and d_{xy}^{u-} under 5% tensile strain is smaller than those in unstrained Co(4 ML)/Gr heterostructure, and the energy difference between opposite spin d_{xy} and $d_{x^2-y^2}$ becomes larger. This decreases the contribution from the matrix element between d_{yz} and d_{z^2} by 0.029 meV, increases the negative contribution from d_{xz} and d_{xy} by 0.042 meV, and increases the contribution from d_{xy} and $d_{x^2-y^2}$ by 0.073 meV. Summing all three terms, a tiny decrease of MAE for Co_1 occurs under 5% tensile strain. The contribution from all four Co atoms makes the MAE of Co/Gr to increase with tensile strain.

The energy difference between $d_{z^2}^{o+}$ and d_{yz}^{u-} of Co_1 in Co/BN also becomes larger compared to Co/Gr. According to Eq. (2), the matrix element difference between the above two orbitals should make the MAE of Co_1 in Co/Gr smaller than that of Co_1 in Co/BN [this can also be seen from Figs. 4(a) and 4(e)]. This explains why the MAE of Co_1 in Co/BN is smaller than that in Co/Gr. It also shows that the orbital overlapping and hybridization between two adjacent layers has large influence on the MAE in multilayer structures [39,47,66].

In contrast to the small positive MAE of Co_2 in unstrained Co(4 ML)/Gr, the MAE of Co_2 in Co(4 ML)/BN has a small negative value. As shown in Figs. 6(c) and 6(d), there are more electrons between Co_1 and Co_2 in Co/Gr than in Co/BN (yellow region between Co_1 and Co_2), which indicates that the bonding between Co_1 and Co_2 in Co/BN is weaker than that in Co/Gr. Similar to the different MAE of Co_1 in Co/BN

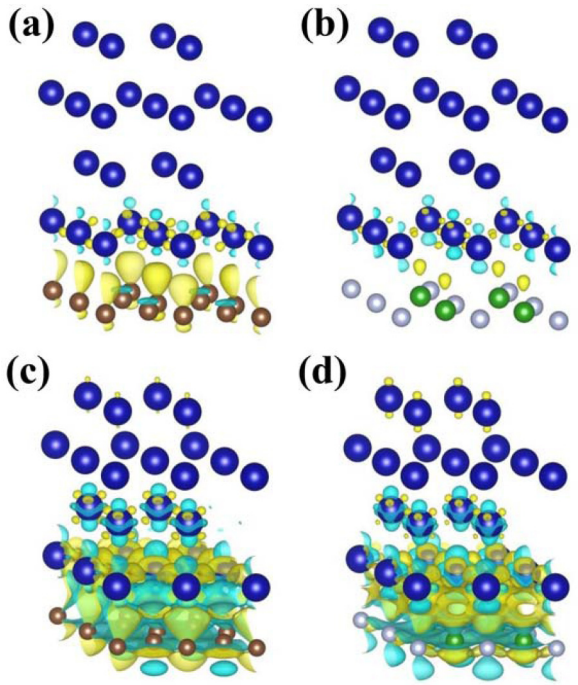

FIG. 6. Differential charge density of (a) and (c) Co(4 ML)/Gr and (b) and (d) Co(4 ML)/BN. The blue, brown, silver, and green ball represent Co, C, N, and B, respectively. Yellow and light blue regions represent charge accumulation and depletion, respectively. The isosurface in (a) and (b) is 0.006 e $Å^{-3}$ and that in (c) and (d) is 0.008 e $Å^{-3}$.

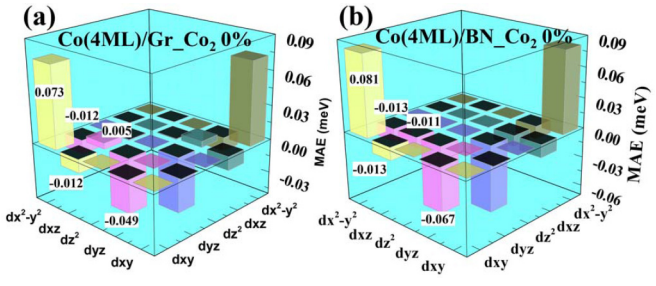

FIG. 7. d-orbital resolved MAE of Co_2 in (a) unstrained Co(4 ML)/Gr and (b) Co(4 ML)/BN, the matrix element differences from each orbital are labeled in the figure.

and Co/Gr, the weaker bonding between Co_1 and Co_2 in Co/BN leads to a smaller MAE of Co_2 as compared to that in Co/Gr (see Fig. 3). Figure 7 shows that the orbital-resolved MAE of Co_2 in unstrained Co(4 ML)/Gr and Co(4 ML)/BN, with the values of MAE from each matrix element difference labeled in the figure. It can be seen that except for the positive contribution from the SOC interaction between d_{xy} and $d_{x^2-y^2}$ orbitals, all other nonzero matrix element differences provide negative contribution to MAE for Co_2 in unstrained Co(4 ML)/BN. Compared to that of Co(4 ML)/Gr, the matrix element differences between d_{xz} and d_{yz} orbitals as well as d_{yz} and d_{z^2} orbitals favor a much higher in-plane anisotropy, which is the main reason why the MAE of Co_2 in Co(4 ML)/BN is a small negative value.

As shown in Fig. 5, the weaker bonding leads to an insensitive DOS of the d_{z^2} orbital of Co_1 in Co(4 ML)/BN with respect to tensile strain, compared to that of Co_1 in Co(4 ML)/Gr. As a result, the contribution to the MAE of Co_1 in Co(4 ML)/BN from the SOC interaction between d_{yz} and d_{z^2} orbitals is nearly unchanged by tensile strain. Figures 4(e) and 4(f) show that the slight increase of the negative contribution from SOC interaction between d_{xz} and d_{xy} as well as the positive contribution from d_{xy} and $d_{x^2-y^2}$ under 5% tensile strain lead to a nearly unchanged MAE of Co_1 in Co(4 ML)/BN.

IV. CONCLUSION

In summary, we provide evidence through first-principles calculations that graphene can greatly enhance the MAE of Co films, while the MAE of Co/BN heterostructure is smaller than that of Co films. Strain is also an effective method for tuning the MAE. A compressive strain increases the distance between the interface Co atom and graphene or BN, diminishing their effect. When the interlayer distance reaches ∼4 Å, the MAE of Co/Gr and Co/BN heterostructures are nearly the same as that of a Co multilayer. On the other hand, a tensile strain can effectively enhance the MAE of Co/Gr and Co/BN heterostructures, up to 48.5% and 80.8% in Co(4 ML)/Gr and Co(4 ML)/BN systems, respectively. The cause of MAE enhancement by tensile strain is the large increase of the positive contribution from hybridization between same spin d_{xy} and $d_{x^2-y^2}$ orbitals of the Co layer surface. Moreover, we find that the contribution from matrix elements between occupied and unoccupied states with opposite spins also plays an important role in Co-based systems. These results provide a promising route for exploiting materials with large perpendicular magnetic anisotropy and low damping constant for spintronic devices.

ACKNOWLEDGMENTS

This work was supported by the 863 Plan Project of Ministry of Science and Technology (MOST, No. 2014AA032904), the MOST National Key Scientific Instrument and Equipment Development Projects (Grant No. 2011YQ120053), the National Natural Science Foundation of China (NSFC, Grants No. 11434014, No. 51229101, and No. 51620105004), the Strategic Priority Research Program (B) of the Chinese Academy of Sciences (CAS) (Grant No. XDB07030200), and the user fund of Wuhan National High Magnetic Field Center (PHMFF2015011). The work was carried out at National Supercomputer Center in Tianjin, and the calculations were performed on TianHe-1 (A).

[1] S. Ikeda, K. Miura, H. Yamamoto, K. Mizunuma, H. Gan, M. Endo, S. Kanai, J. Hayakawa, F. Matsukura, and H. Ohno, Nat. Mater. **9**, 721 (2010).
[2] A. D. Kent, Nat. Mater. **9**, 699 (2010).
[3] L. Berger, Phys. Rev. B **54**, 9353 (1996).
[4] J. C. Slonczewski, J. Magn. Magn. Mater **159**, L1 (1996).
[5] D.-s. Wang, R. Wu, and A. J. Freeman, Phys. Rev. B **48**, 15886 (1993).
[6] A. Lehnert, S. Dennler, P. Błoński, S. Rusponi, M. Etzkorn, G. Moulas, P. Bencok, P. Gambardella, H. Brune, and J. Hafner, Phys. Rev. B **82**, 094409 (2010).
[7] T. Liu, J. Cai, and L. Sun, Aip Adv. **2**, 032151 (2012).
[8] D. Odkhuu, S. H. Rhim, N. Park, and S. C. Hong, Phys. Rev. B **88**, 184405 (2013).
[9] T. Liu, Y. Zhang, J. Cai, and H. Pan, Sci. Rep. **4**, 5895 (2014).
[10] H. Almasi, D. R. Hickey, T. Newhouse-Illige, M. Xu, M. Rosales, S. Nahar, J. Held, K. Mkhoyan, and W. Wang, Appl. Phys. Lett. **106**, 182406 (2015).
[11] J.-H. Kim, J.-B. Lee, G.-G. An, S.-M. Yang, W.-S. Chung, H.-S. Park, and J.-P. Hong, Sci. Rep. **5**, 16903 (2015).
[12] S. Peng, M. Wang, H. Yang, L. Zeng, J. Nan, J. Zhou, Y. Zhang, A. Hallal, M. Chshiev, K. L. Wang *et al.*, Sci. Rep. **5**, 18173 (2015).
[13] W. Skowroński, T. Nozaki, Y. Shiota, S. Tamaru, K. Yakushiji, H. Kubota, A. Fukushima, S. Yuasa, and Y. Suzuki, Appl. Phys. Express **8**, 053003 (2015).
[14] M. Oogane, T. Wakitani, S. Yakata, R. Yilgin, Y. Ando, A. Sakuma, and T. Miyazaki, Jpn. J. Appl. Phys. **45**, 3889 (2006).
[15] A. Barman, S. Wang, O. Hellwig, A. Berger, E. E. Fullerton, and H. Schmidt, J. Appl. Phys. **101**, 09D102 (2007).

[16] S. Gong, C.-G. Duan, Z.-Q. Zhu, and J.-H. Chu, Appl. Phys. Lett. **100**, 122410 (2012).
[17] M. Tsujikawa and T. Oda, Phys. Rev. Lett. **102**, 247203 (2009).
[18] A. S. Zyazin, J. W. van den Berg, E. A. Osorio, H. S. van der Zant, N. P. Konstantinidis, M. Leijnse, M. R. Wegewijs, F. May, W. Hofstetter, C. Danieli *et al.*, Nano Lett. **10**, 3307 (2010).
[19] K. He, J. Chen, and Y. Feng, Appl. Phys. Lett. **99**, 072503 (2011).
[20] S. Mizukami, T. Kubota, F. Wu, X. Zhang, T. Miyazaki, H. Naganuma, M. Oogane, A. Sakuma, and Y. Ando, Phys. Rev. B **85**, 014416 (2012).
[21] W.-G. Wang, M. Li, S. Hageman, and C. Chien, Nat. Mater. **11**, 64 (2012).
[22] P. Ruiz-Díaz, T. R. Dasa, and V. S. Stepanyuk, Phys. Rev. Lett. **110**, 267203 (2013).
[23] F. Donati, L. Gragnaniello, A. Cavallin, F. Natterer, Q. Dubout, M. Pivetta, F. Patthey, J. Dreiser, C. Piamonteze, S. Rusponi *et al.*, Phys. Rev. Lett. **113**, 177201 (2014).
[24] P. V. Ong, N. Kioussis, P. K. Amiri, J. G. Alzate, K. L. Wang, G. P. Carman, J. Hu, and R. Wu, Phys. Rev. B **89**, 094422 (2014).
[25] C.-F. Pai, M.-H. Nguyen, C. Belvin, L. H. Vilela-Leão, D. Ralph, and R. Buhrman, Appl. Phys. Lett. **104**, 082407 (2014).
[26] J. Zhang, C. Franz, M. Czerner, and C. Heiliger, Phys. Rev. B **90**, 184409 (2014).
[27] W. Cong, Z. Tang, X. Zhao, and J. Chu, Sci. Rep. **5**, 9361 (2015).
[28] C. Song, S. Gong, Z. Zhang, H. Mao, Q. Zhao, J. Wang, and H. Xing, J. Phys. D **48**, 485001 (2015).
[29] F. Ibrahim, H. X. Yang, A. Hallal, B. Dieny, and M. Chshiev, Phys. Rev. B **93**, 014429 (2016).
[30] K. Hotta, K. Nakamura, T. Akiyama, T. Ito, T. Oguchi, and A. J. Freeman, Phys. Rev. Lett. **110**, 267206 (2013).
[31] R. Xiao, D. Fritsch, M. D. Kuzmin, K. Koepernik, H. Eschrig, M. Richter, K. Vietze, and G. Seifert, Phys. Rev. Lett. **103**, 187201 (2009).
[32] A. Hallal, H. X. Yang, B. Dieny, and M. Chshiev, Phys. Rev. B **88**, 184423 (2013).
[33] D. Odkhuu, Sci. Rep. **6**, 32742 (2016).
[34] I. G. Rau, S. Baumann, S. Rusponi, F. Donati, S. Stepanow, L. Gragnaniello, J. Dreiser, C. Piamonteze, F. Nolting, S. Gangopadhyay *et al.*, Science **344**, 988 (2014).
[35] X. Ou, H. Wang, F. Fan, Z. Li, and H. Wu, Phys. Rev. Lett. **115**, 257201 (2015).
[36] R. Xiao, D. Fritsch, M. D. Kuzmin, K. Koepernik, M. Richter, K. Vietze, and G. Seifert, Phys. Rev. B **82**, 205125 (2010).
[37] N. Rougemaille, A. N'Diaye, J. Coraux, C. Vo-Van, O. Fruchart, and A. Schmid, Appl. Phys. Lett. **101**, 142403 (2012).
[38] A.-D. Vu, J. Coraux, G. Chen, A. N'Diaye, A. Schmid, and N. Rougemaille, Sci. Rep. **6**, 24783 (2016).
[39] A. Barla, V. Bellini, S. Rusponi, P. Ferriani, M. Pivetta, F. Donati, F. Patthey, L. Persichetti, S. K. Mahatha, M. Papagno *et al.*, ACS nano **10**, 1101 (2016).
[40] H. Yang, A. D. Vu, A. Hallal, N. Rougemaille, J. Coraux, G. Chen, A. K. Schmid, and M. Chshiev, Nano Lett. **16**, 145 (2016).
[41] Y. Tokura and N. Nagaosa, Science **288**, 462 (2000).
[42] J. Haeni, P. Irvin, W. Chang, R. Uecker, P. Reiche, Y. Li, S. Choudhury, W. Tian, M. Hawley, B. Craigo *et al.*, Nature (London) **430**, 758 (2004).
[43] C. Ederer and N. A. Spaldin, Phys. Rev. B **71**, 224103 (2005).
[44] J. A. Heuver, A. Scaramucci, Y. Blickenstorfer, S. Matzen, N. A. Spaldin, C. Ederer, and B. Noheda, Phys. Rev. B **92**, 214429 (2015).
[45] D. Fritsch and C. Ederer, Phys. Rev. B **82**, 104117 (2010).
[46] P. V. Ong, N. Kioussis, D. Odkhuu, P. Khalili Amiri, K. L. Wang, and G. P. Carman, Phys. Rev. B **92**, 020407(R) (2015).
[47] S. Ouazi, S. Vlaic, S. Rusponi, G. Moulas, P. Buluschek, K. Halleux, S. Bornemann, S. Mankovsky, J. Minár, J. B. Staunton *et al.*, Nat. Commun. **3**, 1313 (2012).
[48] G. H. O. Daalderop, P. J. Kelly, and M. F. H. Schuurmans, Phys. Rev. B **50**, 9989 (1994).
[49] G. van der Laan, J. Phys.: Condens. Matter **10**, 3239 (1998).
[50] C. Andersson, B. Sanyal, O. Eriksson, L. Nordström, O. Karis, D. Arvanitis, T. Konishi, E. Holub-Krappe, and J. H. Dunn, Phys. Rev. Lett. **99**, 177207 (2007).
[51] G. Kresse and J. Furthmüller, Phys. Rev. B **54**, 11169 (1996).
[52] G. Kresse and J. Furthmüller, Comput. Mater. Sci. **6**, 15 (1996).
[53] G. Kresse and J. Hafner, Phys. Rev. B **47**, 558 (1993).
[54] J. P. Perdew, K. Burke, and M. Ernzerhof, Phys. Rev. Lett. **77**, 3865 (1996).
[55] P. E. Blöchl, Phys. Rev. B **50**, 17953 (1994).
[56] J. Klimeš, D. R. Bowler, and A. Michaelides, J. Phys.: Condens. Matter **22**, 022201 (2010).
[57] J. Klimeš, D. R. Bowler, and A. Michaelides, Phys. Rev. B **83**, 195131 (2011).
[58] T. Ohta, A. Bostwick, T. Seyller, K. Horn, and E. Rotenberg, Science **313**, 951 (2006).
[59] M. Corso, W. Auwärter, M. Muntwiler, A. Tamai, T. Greber, and J. Osterwalder, Science **303**, 217 (2004).
[60] M. Topsakal and S. Ciraci, Phys. Rev. B **81**, 024107 (2010).
[61] Y. Yang, W. Ren, M. Stengel, X. H. Yan, and L. Bellaiche, Phys. Rev. Lett. **109**, 057602 (2012).
[62] V. M. Karpan, G. Giovannetti, P. A. Khomyakov, M. Talanana, A. A. Starikov, M. Zwierzycki, J. van den Brink, G. Brocks, and P. J. Kelly, Phys. Rev. Lett. **99**, 176602 (2007).
[63] X. Wang, D.-s. Wang, R. Wu, and A. Freeman, J. Magn. Magn. Mater **159**, 337 (1996).
[64] D. Li, C. Barreteau, and A. Smogunov, Phys. Rev. B **93**, 144405 (2016).
[65] D.-s. Wang, R. Wu, and A. J. Freeman, Phys. Rev. B **47**, 14932 (1993).
[66] H. X. Yang, M. Chshiev, B. Dieny, J. H. Lee, A. Manchon, and K. H. Shin, Phys. Rev. B **84**, 054401 (2011).